Theta-Band Temporal Interference Stimulation Targeting the dACC Modulates Neural Gain of Prediction Error Encoding

Authors: Yatong Wen[a,b,c], Mo Wang[d,e], Xinwen Dong[a], Mateusz Gola[f,g], Quanying Liu[d], Yiheng Tu[a,b*], Yonghui Li[a,b*]

[a] State Key Laboratory of Cognitive Science and Mental Health, Institute of Psychology, Chinese Academy of Sciences, Beijing, China

[b] Department of Psychology, University of Chinese Academy of Sciences, Beijing, China

[c] Department of Neuroscience, Karolinska Institutet, Stockholm 171 65, Sweden

[d] Department of Biomedical Engineering, Southern University of Science and Technology, Shenzhen 518055, China

[e] Department of Computer Science, University of Warwick, Coventry, United Kingdom

[f] Institute of Psychology, Polish Academy of Sciences, Warsaw, Poland

[g] Swartz Center for Computational Neuroscience, Institute for Neural Computations, University of California, San Diego, CA, USA

* Correspondence:

Yiheng Tu, State Key Laboratory of Cognitive Science and Mental Health, Institute of Psychology, Chinese Academy of Sciences, No.16 Lincui Road, Chaoyang District, Beijing 100101, China. Email: tuyh@psych.ac.cn

and

Yonghui Li, State Key Laboratory of Cognitive Science and Mental Health, Institute of Psychology, Chinese Academy of Sciences, No.16 Lincui Road, Chaoyang District, Beijing 100101, China. Email: liyonghui@psych.ac.cn

Keywords: temporal interference stimulation; dorsal anterior cingulate cortex; prediction error; feedback-related negativity; EEG

Abstract

Background: Prediction error (PE) signals encode discrepancies between expected and actual outcomes and are linked to medial frontal theta dynamics in the dorsal anterior cingulate cortex (dACC). However, causal evidence that dACC theta mechanisms contribute to PE gain in humans remains limited. Transcranial temporal interference stimulation (tTIS) enables non-invasive modulation of deep cortical targets and provides a strategy to probe dACC theta circuitry.

Objective: To determine whether theta-band tTIS targeting the dACC modulates the neural gain of prediction error encoding during reward processing.

Methods: Thirty-four participants with elevated food addiction-related symptoms were randomized in a single-blind, sham-controlled pre-post design to active theta-band tTIS or sham stimulation. Under satiety, participants completed a food incentive delay task while EEG was recorded before and after stimulation. Feedback-related negativity (FRN) was analyzed at mean and single-trial levels using mixed-effects models with behavioral and Rescorla-Wagner model-derived prediction errors. Stimulus-preceding negativity (SPN) indexed anticipatory processing.

Results: Theta-band tTIS selectively modulated feedback-stage prediction error encoding. It altered the trial-level FRN–prediction error slope, with pre-to-post changes differing between groups for both behavioral ($\beta = 1.74$, $p = .049$) and model-derived prediction errors ($\beta = 1.77$, $p = .048$). At the mean ERP level, FRN became more negative after active stimulation ($t_{16} = 2.75$, $p = .014$), whereas SPN was unaffected.

Conclusion: Theta-band tTIS targeting the dACC modulates neural sensitivity to prediction errors during reward feedback, providing causal evidence that medial frontal theta dynamics regulate the neural gain of prediction error encoding.

Introduction

Prediction error signals guide adaptive learning by encoding discrepancies between expected and actual outcomes [1–3]. Converging electrophysiological and neuroimaging

evidence indicates that medial frontal theta-band dynamics have been implicated in this process [4], with the dorsal anterior cingulate cortex (dACC) serving as a key generator of feedback-related prediction error activity [5]. Neuronal recordings demonstrate that dACC ensembles dynamically update firing patterns in response to outcome deviations [6], whereas synchronized theta oscillations are thought to coordinate performance monitoring across prefrontal networks [4] and support adaptive behavioral adjustments [7]. Together, these converging neuronal and oscillatory findings implicate dACC theta dynamics as a candidate mechanism regulating the neural gain of prediction error encoding in humans. However, causal tests of these dACC-centered, frequency-specific oscillatory mechanisms in humans remain limited.

Conventional non-invasive stimulation approaches provide limited access to deep medial frontal cortex such as the dACC. Transcranial alternating current stimulation (tACS) demonstrates frequency-dependent modulation of cortical rhythms [8–10]. Phase- and state-dependent stimulation can also modulate oscillatory dynamics and influence neural gain in a behaviorally relevant manner [11,12]. However, these approaches predominantly influence superficial cortical regions and are poorly suited for selectively engaging deeper medial frontal structures. Invasive recordings obtained during deep brain stimulation (DBS) procedures provide rare human evidence linking dACC activity to prediction error processing [13]. However, DBS is confined to clinical contexts and does not permit controlled frequency-specific interrogation of oscillatory mechanisms. A non-invasive method capable of selectively modulating deep cortical oscillations at a defined frequency would therefore provide critical mechanistic insight into whether medial frontal theta dynamics regulate prediction error gain.

Transcranial temporal interference stimulation (tTIS) enables non-invasive modulation of deep brain regions by generating a low-frequency envelope through the interaction of two high-frequency currents [14]. Biophysical modeling suggests that temporal interference can concentrate envelope modulation in deep structures while minimizing stimulation of overlying cortex [15]. Emerging human evidence further supports its capacity to modulate deep oscillatory circuits [16,17]. This approach enables causal testing of deep, frequency-specific

modulation of dACC activity during prediction error encoding.

Here, we tested whether theta-band tTIS targeting the dACC modulates the neural gain of prediction error encoding during reward processing. The experiment was conducted in individuals exhibiting elevated reward expectancy bias, operationalized as elevated food addiction-related symptoms assessed using validated questionnaires [18,19]. Prior work indicates that this expectancy bias persists even under satiety and is associated with reduced sensitivity to outcome discrepancies [18]. Such persistent expectancy bias provides a model in which deviations between expected and actual outcomes may be informative for probing prediction error dynamics. In this context, unfavorable (negative) prediction errors provide a sensitive index of updating; analyses therefore focused on negative prediction error trials. We hypothesized that theta-band deep modulation would alter the coupling between electrophysiological indices of dACC activity and trial-by-trial prediction errors.

Materials and methods

Participants

Thirty-four participants with elevated food addiction-related symptoms were recruited (15 males, 19 females). Symptoms were assessed using the Yale Food Addiction Scale (YFAS), with inclusion criteria of a YFAS symptom score $\geqslant$ 3 and BMI $\geqslant$ 25, consistent with prior studies [20–22]. The mean age of the sample was 25.32 ± 4.64 years (range: 19–39 years), and the mean body mass index (BMI) was 27.75 ± 5.05 kg/m². Exclusion criteria included a history of neurological or psychiatric disorders, current use of psychoactive medication, epilepsy or seizure history, metal implants in the head, dermatological conditions affecting the scalp, pregnancy, or contraindications to non-invasive brain stimulation.

All participants had normal or corrected-to-normal vision and provided written informed consent in accordance with the Declaration of Helsinki. The study protocol was approved by the Ethics Committee of the Institute of Psychology, Chinese Academy of Sciences on October 31, 2023 (No. H23113).

Participants were randomly assigned to the active tTIS group (n = 17) or the sham stimulation group (n = 17). Participants consumed lunch before testing and refrained from

further caloric intake. Hunger levels were assessed immediately before the experiment using a 10-point visual scale, and all participants reported hunger ratings below 5. Participants received a base payment of ¥200–¥230, with an additional performance-based bonus of up to ¥15.

Study design and procedure

The study employed a mixed 2 × 2 design with Group (active tTIS vs. sham stimulation) as a between-subject factor and Phase (pre- vs. post-stimulation) as a within-subject factor. The experiment comprised pretest, stimulation, and posttest phases. EEG was recorded during the 150-trial pretest and posttest, but not during stimulation. Before the main experiment, participants completed a practice session to familiarize themselves with the task and were required to achieve at least 80% accuracy before proceeding. All trials involved food rewards represented by standardized food images matched on arousal, pleasantness, and familiarity (Supplementary Section 1; Table S1). The overall experimental timeline is illustrated in Figure 1, and the task structure is shown in Figure 2.

[Insert Figure 1 here]

Incentive Delay Task

Reward processing was assessed using a modified Incentive Delay Task (IDT) adapted from Knutson et al. [23], focusing on food reward outcomes. Each trial began with a cue indicating the probability of receiving a food reward (high: 80%; low: 20%), followed by a response phase in which participants indicated whether they expected to receive a reward (yes/no) using a binary button press ("F" or "J"). After a 2000-ms delay, feedback was presented for 1500 ms. Reward feedback consisted of the presentation of a food image (reward) or a scrambled image (no reward). Inter-trial intervals varied between 350 and 650 ms. Behavioral outcomes included reaction times and reward prediction rates under high- and low-probability conditions. These trial-wise expectation–outcome combinations were used to derive behavioral prediction errors coded as −1 (worse-than-expected), 0 (expected), and +1 (better-than-expected).

[Insert Figure 2 here]

Electroencephalogram (EEG) recording and processing

Continuous EEG was recorded using a 64-channel system (Neuracle NeuSen.W 64; Neuracle, Changzhou, China), referenced to CPz with AFz as ground. Signals were sampled at 1000 Hz, electrode impedances were kept below 10 kΩ, and data were rereferenced offline to the average of the bilateral mastoids (M1/M2). Analyses focused on two ERP components: feedback-related negativity (FRN), indexing feedback evaluation, and stimulus-preceding negativity (SPN), indexing anticipatory processing.

EEG preprocessing was conducted in EEGLAB/ERPLAB using custom MATLAB scripts. Data were band-pass filtered using zero-phase finite impulse response filters (FRN: 0.1–30 Hz; SPN: low-pass filter at 30 Hz), epoched relative to feedback onset, and cleaned using automated rejection, manual inspection, and independent component analysis (ICA; runica algorithm) to remove ocular and muscle artifacts. Trials with residual artifacts exceeding ±100 μV were automatically rejected. SPN epochs were extracted from −2000 to 500 ms (baseline: −2000 to −1800 ms), and FRN epochs from −200 to 1000 ms (baseline: −200 to 0 ms). Single-trial amplitudes were extracted for mixed-effects analyses, and grand averages were computed for visualization.

Transcranial Temporal Interference Stimulation

tTIS was delivered using an interferential neuromodulation system (Soterix Medical Inc.) targeting the dACC. Ag/AgCl electrodes (1.2 cm diameter; contact area = 1.13 cm^2) were placed according to an optimized unilateral montage [24] (Supplementary Section 2). Target coordinates (MNI: −5, 34, 30) were derived from a prior neuromodulation study [25] and verified using FSL and MNI–Talairach conversion tools (see URL in Supplementary Section 2). Electrodes were attached using conductive gel and secured to ensure stable contact.

Four electrodes were used (AF3 positive, Fz negative, CP3 positive, F7 negative). Finite-element simulations estimated the temporal interference envelope distribution and confirmed field intensity in the dACC target (Figure 3). Stimulation used two high-frequency currents (2000 and 2005 Hz) producing a 5-Hz theta-band envelope. Current intensity was 1.6 mA (peak-to-baseline) per electrode for 20 minutes. Active stimulation included gradual ramp-in and ramp-out periods, whereas sham stimulation consisted of a 30-s ramp-up and ramp-down

without sustained stimulation.

[Insert Figure 3 here]

Statistical analysis

Trial-level analysis of prediction error

Single-trial FRN amplitudes were analyzed using linear mixed-effects models (LME; MATLAB fitlme) [26]. Behavioral prediction errors (PE) were coded as −1 (worse-than-expected), 0 (expected), and +1 (better-than-expected). The model included fixed effects of PE, Group (active vs. sham), Phase (pre vs. post), and their interactions: FRN amplitude ~ PE × Group × Phase + (1 + PE | subject). If the maximal model failed to converge, a random-intercept model (1 | subject) was used. Fixed effects were evaluated using Wald z tests (two-tailed). Significant interactions were followed by simple-effects analyses across PE levels. Each session consisted of 150 trials. Behavioral negative prediction errors occurred relatively infrequently, yielding on average approximately 22 trials per participant per phase (range: 8–67).

Computational estimation of trial-level prediction errors

Given the limited number of trials for categorical negative prediction errors, model-derived prediction errors (PE_RW) were additionally estimated using a Rescorla–Wagner computational model [2] fitted to trial-wise behavioral data (Supplementary Section 3). This approach provided a continuous estimate of trial-wise prediction error and incorporated a larger proportion of trials (approximately 84 trials per phase). Single-trial FRN amplitudes were analyzed using an analogous LME model: FRN amplitude ~ PE_RW × Group × Phase + (1 + PE_RW | subject). If the maximal model failed to converge, a simplified random-intercept model (1 | subject) was used. Follow-up analyses examined Group × Phase effects across PE_RW sign (PE_RW < 0, PE_RW = 0, PE_RW > 0).

ERP and behavioral analyses

Mean ERP and behavioral outcomes were analyzed using repeated-measures ANOVAs with Group (active vs. sham) as a between-subject factor and Phase (pre vs. post) as a within-subject factor. FRN amplitude was quantified as peak negativity within the 250–350 ms

window at FCz, and SPN amplitude as mean voltage within the −200 to 0 ms window preceding feedback onset. Difference waves (no reward − reward) were used for visualization. For condition-level ERP analyses, negative prediction error trials were defined based on expectation–outcome mismatch (PE = −1). Greenhouse–Geisser corrections were applied where appropriate, with statistical significance set at $p < .05$.

Power analysis and blinding

Sample size was determined a priori using G*Power (version 3.1) [27] for a repeated-measures ANOVA testing the Group × Phase interaction. Assuming a medium effect size ($f = 0.25$), $\alpha = .05$, and power = 0.80, the required sample was 34 participants (17 per group).

Integrity of the Blind

This study employed a single-blind design in which participants were unaware of the stimulation condition (active vs. sham). Due to technical constraints inherent to the tTIS setup, the experimenter administering stimulation was not blinded. To assess the integrity of blinding, participants were asked after each session to indicate whether they believed they had received active or sham stimulation. Blinding success was evaluated by comparing guessing accuracy against chance level (50%). Participants were unable to reliably identify the stimulation condition, with guessing accuracy not differing from chance, indicating preserved participant-level blinding.

Results

Demographic characteristics

Thirty-four participants were randomized to the active tTIS group (n = 17) or the sham stimulation group (n = 17). Demographic and clinical characteristics are summarized in Table S2. The two groups did not differ in Yale Food Addiction Scale scores, body mass index, age, education level, household income, or hunger ratings (all $p > .05$). Mild transient sensations (e.g., headache or tingling) were reported more frequently in the active group, but no participant reported lasting discomfort. Participants were unable to reliably identify stimulation condition (Table S3).

Trial-level encoding of behavioral prediction errors

Single-trial FRN amplitudes scaled significantly with PE ($\beta = 2.66$, $SE = 0.44$, $z = 5.99$, $p = 2.06 \times 10^{-9}$), indicating robust trial-level sensitivity of FRN amplitudes to prediction errors during reward feedback. Significant PE × Phase ($\beta = -1.69$, $SE = 0.61$, $z = -2.76$, $p = .006$) and PE × Group interactions ($\beta = -1.51$, $SE = 0.63$, $z = -2.39$, $p = .017$) were observed. Importantly, a significant Group × Phase × PE interaction ($\beta = 1.74$, $SE = 0.89$, $z = 1.97$, $p = .049$) indicated that pre-to-post changes in the trial-level FRN–PE slope differed between the active and sham groups.

Figure 4 illustrates the trial-level relationship between FRN amplitude and prediction errors across groups and phases, based on fitted relationships from the mixed-effects model. Follow-up contrasts indicated that the Group × Phase effect was most pronounced for unfavorable outcomes (PE = −1; $\beta = -3.45$, $SE = 0.97$, $z = -3.56$, $p = 3.70 \times 10^{-4}$; Table S4). Subject-level FRN–PE slopes are provided in Supplementary Figure S1 for descriptive purposes.

[Insert Figure 4 here]

Trial-level encoding of model-based prediction errors

Single-trial FRN amplitudes scaled significantly with PE_RW ($\beta = 2.94$, $SE = 0.45$, $z = 6.53$, $p = 6.62 \times 10^{-11}$), indicating robust trial-level sensitivity of FRN amplitudes to model-derived prediction errors. Significant PE_RW × Group ($\beta = -1.42$, $SE = 0.64$, $z = -2.21$, $p = .027$) and PE_RW × Phase interactions ($\beta = -1.04$, $SE = 0.62$, $z = -1.69$, $p = .092$) were observed. Critically, a significant Group × Phase × PE_RW interaction ($\beta = 1.77$, $SE = 0.90$, $z = 1.98$, $p = .048$) indicated differential pre-to-post changes in the trial-level FRN–PE_RW slope between groups.

Figure 5 illustrates the trial-level relationship between FRN amplitude and model-derived prediction errors across groups and phases, based on fitted relationships from the mixed-effects model. Follow-up contrasts indicated that the Group × Phase effect was most pronounced for negative prediction errors (PE_RW < 0; $\beta = -2.46$, $SE = 0.56$, $z = -4.36$, $p = 1.29 \times 10^{-5}$; Table S5). Subject-level slopes are provided in Supplementary Figure S2 for

descriptive purposes.

[Insert Figure 5 here]

ERP indices of feedback and anticipation

FRN

To complement the trial-level mixed-effects analyses, condition-averaged FRN amplitudes were additionally examined for negative prediction errors (PE = −1; PE_RW < 0). This follow-up was guided by the trial-level localization analyses indicating that stimulation-related modulation was most pronounced for unfavorable outcomes (Tables S4–S5). These analyses yielded a consistent pattern of increased post-stimulation FRN negativity in the active group, with no corresponding change in the sham group (Figures S3–S4; Supplementary Section 6 for full statistics).

Figure 6 shows grand-average FRN waveforms and scalp topographies elicited by food reward outcomes in the active and sham groups before and after stimulation. FRN was observed as a fronto-central negative deflection peaking around 300 ms after feedback. Baseline FRN amplitudes did not differ between groups during the pre-stimulation phase (t_{32} = −0.35, p = .730, d = .12). A significant main effect of phase was observed ($F_{1,32}$ = 6.13, p = .019, η_p^2 = .16), along with a trend-level Group × Phase interaction ($F_{1,32}$ = 3.86, p = .058, η_p^2 = .12). Follow-up analyses indicated that FRN amplitudes became significantly more negative after stimulation in the active group (t_{16} = 2.75, p = .014, d = .67), consistent with the trial-level findings, whereas no significant change was observed in the sham group (t_{16} = 0.44, p = .67, d = .11) (Figure 8A).

[Insert Figure 6 here]

SPN

SPN waveforms and scalp distributions are shown in Figure 7. Baseline SPN amplitudes were comparable between groups (t_{32} = 0.60, p = .55, d = .21). No main effects of Group or Phase, nor a Group × Phase interaction, were observed (all p > .80). Quantitative SPN results are summarized in Figure 8B.

[Insert Figure 7 here]

[Insert Figure 8 here]

Behavioral data

Behavioral performance during the incentive delay task was analyzed to examine whether stimulation-related neural effects were accompanied by behavioral changes. Reaction times showed a significant main effect of Phase ($F_{1,32}$ = 10.73, p = .003, η_p^2 = .25), with faster responses post-stimulation, but no main effect of Group or Group × Phase interaction (both p > .05). Reward prediction rates did not differ as a function of Group, Phase, or their interaction for either high- or low-probability cues (all p > .05).

Discussion

To our knowledge, the present study provides the first causal evidence that theta-band tTIS targeting the dACC modulates feedback-stage prediction error encoding during reward processing. In a randomized sham-controlled pre-post design, active stimulation altered the trial-level coupling between FRN amplitudes and prediction errors derived from both behavioral expectation-outcome mismatch and a Rescorla-Wagner computational model. Complementary ERP analyses converged with these findings, showing increased FRN negativity following active stimulation, whereas anticipatory activity indexed by SPN remained unchanged. Together, these results suggest that theta-band tTIS preferentially modulated the neural gain of prediction error encoding during feedback processing.

Trial-level modulation of prediction error gain

The primary empirical contribution lies in the trial-level analyses linking FRN amplitudes to prediction errors. Single-trial FRN amplitudes scaled reliably with both categorical behavioral prediction errors and continuous prediction errors estimated from a Rescorla-Wagner computational model, indicating robust neural tracking of outcome discrepancies during feedback evaluation.

Critically, theta-band tTIS significantly modulated this relationship, as reflected by Group × Phase × prediction error interactions observed in the mixed-effects models. These results indicate that stimulation altered the strength of trial-level FRN–prediction error coupling across

sessions, with differential pre-to-post changes between the active and sham groups. Follow-up contrasts further localized this modulation primarily to unfavorable outcomes (PE = −1; PE_RW < 0), consistent with previous findings showing stronger FRN responses to negative feedback during outcome evaluation [1,28].

Together, these findings suggest that theta-band tTIS altered the gain of prediction error encoding, as reflected in the sensitivity of FRN amplitudes to trial-by-trial outcome discrepancies, rather than producing a nonspecific shift in feedback-evoked activity. Subject-level slopes showed a similar numerical pattern but did not reach statistical significance. The primary inference therefore derives from the trial-level mixed-effects models, which leverage all available observations and provide greater statistical sensitivity to detect changes in this coupling.

dACC theta modulation as a candidate mechanism

The present findings are consistent with the established role of the dACC in signaling outcome discrepancies and coordinating adaptive control through theta-band dynamics [7,29]. Converging electrophysiological and neuroimaging evidence indicates that medial frontal theta activity supports feedback evaluation, error monitoring, and adaptive control following unfavorable outcomes [7,30,31]. The FRN, a fronto-central negative deflection observed during outcome evaluation, has been closely linked to medial frontal theta activity and is widely interpreted as an electrophysiological index of prediction error processing [1,3,4].

Within this framework, the observed stimulation effects suggest that theta-band tTIS influenced the responsivity of dACC-centered evaluative circuits to deviations between expected and actual outcomes. Because the stimulation protocol generated a theta-frequency envelope targeting the dACC, the enhanced coupling between FRN amplitudes and prediction errors is consistent with the hypothesis that medial frontal theta dynamics regulate the neural gain of prediction error encoding.

However, the present EEG data do not allow direct differentiation between local modulation of dACC theta activity and indirect effects mediated through distributed cingulo-frontal networks. Given the dense anatomical and functional connectivity of the dACC, it is

likely that stimulation influenced a broader feedback-evaluation network rather than a single isolated cortical node. Thus, the present findings are best interpreted as evidence that theta-band tTIS influenced prediction error encoding within a dACC-centered network, rather than indicating exclusive modulation of a single cortical site. Although electric-field modeling indicated peak envelope amplitude in medial frontal regions, the findings are best interpreted as network-level rather than strictly focal modulation. Future work combining tTIS with source-resolved EEG, connectivity analyses, or multimodal imaging will be important for clarifying the network-level mechanisms underlying these effects.

Dissociation between feedback evaluation and anticipatory processing

Theta-band tTIS exerted stage-specific effects on reward processing. Whereas stimulation reliably altered feedback-stage FRN–prediction error coupling, anticipatory activity indexed by SPN remained unchanged. Because SPN has been associated with anticipatory attention, motivational engagement, and preparatory processes occurring prior to feedback delivery [32–34], this dissociation suggests that theta-band modulation of dACC-centered networks preferentially influences evaluative computations engaged during outcome processing rather than anticipatory preparatory processes [1,3,5,35].

This stage specificity also aligns with previous observations of an imbalanced anticipatory–feedback profile in food addiction under satiety, characterized by relatively elevated anticipatory signals but reduced feedback-based updating relative to healthy controls [18]. Within this context, the present findings suggest that a single session of theta-band tTIS may acutely modulate feedback updating mechanisms that support prediction error signaling, without substantially altering anticipatory expectancy signals. Repeated stimulation or alternative stimulation parameters may be required to influence anticipatory components such as SPN.

Implications for non-invasive modulation of deep reward-monitoring circuits

tTIS has emerged as a promising non-invasive approach for modulating deep cortical structures that are difficult to access with conventional stimulation techniques [14,15]. Although early studies primarily relied on computational modeling or indirect behavioral

outcomes, recent human work has begun to provide evidence for functional modulation of targeted circuits [16,17]. By demonstrating that theta-band tTIS altered trial-level FRN–prediction error coupling, the present study extends this literature beyond mean-amplitude ERP effects and illustrates how tTIS can be used to causally probe prediction-error-related computations in deep medial frontal circuits.

More broadly, these findings support the use of tTIS as a mechanistic tool for interrogating deep reward-monitoring circuits in humans. They also motivate future work to test whether repeated stimulation can produce more sustained changes in prediction error signaling, downstream behavioral adaptation, and potentially clinically relevant reward-learning phenotypes.

Limitations and future directions

Several limitations should be acknowledged. First, although the sample size was sufficient to detect the primary interaction effects and trial-level mixed-effects models improved sensitivity by leveraging all available observations, statistical power may have been limited for detecting subtler between-group differences in subject-level summary indices such as individual FRN–prediction error slopes [26]. Second, only short-term effects of a single stimulation session were assessed; future studies should examine whether repeated stimulation produces sustained changes in prediction error sensitivity and related behavioral adaptation. Third, although the stimulation target was defined in the dACC, the present EEG data do not permit precise source-level attribution, and stimulation may have influenced a broader cingulo-frontal network. Finally, reward processing depends on distributed circuits beyond the dACC, including striatal and prefrontal systems [36]; combining tTIS with multimodal imaging or connectivity analyses may help clarify the network-level mechanisms underlying the present effects. Although mild sensations were more frequently reported in the active condition, participants were unable to reliably identify stimulation condition, suggesting that expectancy-related confounds are unlikely to account for the observed effects.

Conclusion

Theta-band tTIS targeting the dACC modulated feedback-stage prediction error encoding

during reward processing in participants from the general population with elevated food addiction-related symptoms. Trial-level mixed-effects analyses showed altered FRN–prediction error coupling for both behavioral and model-derived prediction errors, with effects localized primarily to unfavorable outcomes. Complementary ERP analyses converged with these findings, showing enhanced FRN negativity after active stimulation without changes in SPN. Given that prediction error encoding reflects a domain-general computational process, these findings are consistent with a domain-general role of prediction error encoding in outcome evaluation. Together, these results demonstrate that medial frontal theta dynamics contribute to the neural gain of prediction error encoding and support tTIS as a promising tool for probing deep, frequency-specific computations in dACC-centered reward-monitoring circuits.

Acknowledgments

This work was supported by the Chinese National Programs for Brain Science and Brain-like Intelligence Technology (Grant No. 2021ZD0202104) and the International Cooperation and Exchange Program of the National Natural Science Foundation of China (Grant No. 32161133004).

CRediT authorship contribution statement

Yatong Wen: Conceptualization, Methodology, Investigation, Formal analysis, Data curation, Visualization, Writing – original draft. **Yonghui Li:** Funding acquisition, Supervision, Writing – review & editing. **Yiheng Tu:** Funding acquisition, Supervision, Writing – review & editing. **Mo Wang:** Methodology, Software. **Xinwen Dong:** Validation, Writing – review & editing. **Mateusz Gola:** Writing – review & editing. **Quanying Liu:** Methodology.

Declaration of competing interest

The authors declare that they have no known competing financial interests or personal relationships that could have appeared to influence the work reported in this paper.

Preprint

A preprint version of this manuscript has been deposited on the bioRxiv preprint server and is disclosed in accordance with journal policy. DOI: 10.64898/2025.12.20.695275.

Data availability

De-identified behavioral data and derived ERP measures supporting the findings of this study are available at OSF: https://doi.org/10.17605/OSF.IO/N28A6. Analysis scripts will be made publicly available upon publication.

Declaration of generative AI and AI-assisted technologies in the manuscript preparation process

During the preparation of this manuscript, the authors used ChatGPT (OpenAI) for language editing and improving readability. The authors reviewed and edited all content to ensure accuracy and take full responsibility for the final manuscript.

References

[1] Holroyd CB, Coles MGH. The neural basis of human error processing: Reinforcement learning, dopamine, and the error-related negativity. Psychological Review 2002;109:679–709. https://doi.org/10.1037/0033-295X.109.4.679.

[2] Rescorla RA, Wagner AR. A theory of Pavlovian conditioning: Variations in the effectiveness of reinforcement and nonreinforcement. In: Black AH, Prokasy WF, editors. Classical Conditioning II: Current Research and Theory, New York: Appleton-Century-Crofts; 1972, p. 64–99.

[3] Sambrook TD, Goslin J. A neural reward prediction error revealed by a meta-analysis of ERPs using great grand averages. Psychological Bulletin 2015;141:213–35. https://doi.org/10.1037/bul0000006.

[4] Cavanagh JF, Frank MJ. Frontal theta as a mechanism for cognitive control. Trends in Cognitive Sciences 2014;18:414–21. https://doi.org/10.1016/j.tics.2014.04.012.

[5] Holroyd CB, Nieuwenhuis S, Yeung N, Nystrom L, Mars RB, Coles MGH, et al. Dorsal anterior cingulate cortex shows fMRI response to internal and external error signals. Nat Neurosci 2004;7:497–8. https://doi.org/10.1038/nn1238.

[6] Hyman JM, Holroyd CB, Seamans JK. A Novel Neural Prediction Error Found in Anterior Cingulate Cortex Ensembles. Neuron 2017;95:447-456.e3. https://doi.org/10.1016/j.neuron.2017.06.021.

[7] Womelsdorf T, Johnston K, Vinck M, Everling S. Theta-activity in anterior cingulate cortex predicts task rules and their adjustments following errors. Proc Natl Acad Sci USA 2010;107:5248–53. https://doi.org/10.1073/pnas.0906194107.

[8] Spampinato D, Avci E, Rothwell J, Rocchi L. Frequency-dependent modulation of cerebellar excitability during the application of non-invasive alternating current stimulation. Brain Stimulation 2021;14:277–83. https://doi.org/10.1016/j.brs.2021.01.007.

[9] Kanai R, Paulus W, Walsh V. Transcranial alternating current stimulation (tACS) modulates cortical excitability as assessed by TMS-induced phosphene thresholds. Clinical Neurophysiology 2010;121:1551–4. https://doi.org/10.1016/j.clinph.2010.03.022.

[10] Onoda K, Kawagoe T, Zheng H, Yamaguchi S. Theta band transcranial alternating current stimulations modulates network behavior of dorsal anterior cingulate cortex. Sci Rep 2017;7:3607. https://doi.org/10.1038/s41598-017-03859-7.

[11] Khademi F, Royter V, Gharabaghi A. State-dependent brain stimulation: Power or phase? Brain Stimulation 2019;12:296–9. https://doi.org/10.1016/j.brs.2018.10.015.

[12] Myatt JL, Toth R, Denison T, Grennan I, McNamara CG, Stagg CJ, et al. Modulation of motor cortical theta and gamma oscillations using phase-targeted, closed-loop optogenetic stimulation of local excitatory and inhibitory neurons. Brain Stimulation 2026;19:103034. https://doi.org/10.1016/j.brs.2026.103034.

[13] Weiss AR, Gillies MJ, Philiastides MG, Apps MA, Whittington MA, FitzGerald JJ, et al. Dorsal Anterior Cingulate Cortices Differentially Lateralize Prediction Errors and Outcome Valence in a Decision-Making Task. Front Hum Neurosci 2018;12:203. https://doi.org/10.3389/fnhum.2018.00203.

[14] Grossman N, Bono D, Dedic N, Kodandaramaiah SB, Rudenko A, Suk H-J, et al. Noninvasive Deep Brain Stimulation via Temporally Interfering Electric Fields. Cell 2017;169:1029-1041.e16. https://doi.org/10.1016/j.cell.2017.05.024.

[15] Mirzakhalili E, Barra B, Capogrosso M, Lempka SF. Biophysics of Temporal Interference Stimulation. Cell Syst 2020;11:557-572.e5. https://doi.org/10.1016/j.cels.2020.10.004.

[16] Violante IR, Alania K, Cassarà AM, Neufeld E, Acerbo E, Carron R, et al. Non-invasive temporal interference electrical stimulation of the human hippocampus. Nat Neurosci 2023;26:1994–2004. https://doi.org/10.1038/s41593-023-01456-8.

[17] Wessel MJ, Beanato E, Popa T, Windel F, Vassiliadis P, Menoud P, et al. Noninvasive theta-burst stimulation of the human striatum enhances striatal activity and motor skill learning. Nat Neurosci 2023;26:2005–16. https://doi.org/10.1038/s41593-023-01457-7.

[18] Wen Y, Zeng Y, Zhou X, Gola M, Dong X, Li Y. Satiety modulates reward processing in food addiction: Evidence from event-related potentials. Appetite 2026;219:108395. https://doi.org/10.1016/j.appet.2025.108395.

[19] Lei W, Liu K, Chen G, Tolomeo S, Liu C, Peng Z, et al. Blunted reward prediction error signals in internet gaming disorder. Psychol Med 2022;52:2124–33. https://doi.org/10.1017/S003329172000402X.

[20] Gearhardt AN, Corbin WR, Brownell KD. Preliminary validation of the Yale Food Addiction Scale. Appetite 2009;52:430–6. https://doi.org/10.1016/j.appet.2008.12.003.

[21] Gearhardt AN, Corbin WR, Brownell KD. Development of the Yale Food Addiction Scale Version 2.0. Psychol Addict Behav 2016;30:113–21. https://doi.org/10.1037/adb0000136.

[22] Gearhardt AN, Boswell RG, White MA. The association of "food addiction" with disordered eating and body mass index. Eating Behaviors 2014;15:427–33. https://doi.org/10.1016/j.eatbeh.2014.05.001.

[23] Knutson B, Fong GW, Adams CM, Varner JL, Hommer D. Dissociation of reward anticipation and outcome with event-related fMRI: Neuroreport 2001;12:3683–7. https://doi.org/10.1097/00001756-200112040-00016.

[24] Wang M, Lou K, Liu Z, Wei P, Liu Q. Multi-objective optimization via evolutionary algorithm (MOVEA) for high-definition transcranial electrical stimulation of the human brain. Neuroimage 2023;280:120331. https://doi.org/10.1016/j.neuroimage.2023.120331.

[25] Yaakub SN, White TA, Roberts J, Martin E, Verhagen L, Stagg CJ, et al. Transcranial focused ultrasound-mediated neurochemical and functional connectivity changes in deep cortical regions in humans. Nat Commun 2023;14:5318. https://doi.org/10.1038/s41467-

023-40998-0.

[26] Baayen RH, Davidson DJ, Bates DM. Mixed-effects modeling with crossed random effects for subjects and items. Journal of Memory and Language 2008;59:390–412. https://doi.org/10.1016/j.jml.2007.12.005.

[27] Faul F, Erdfelder E, Lang A-G, Buchner A. G*Power 3: A flexible statistical power analysis program for the social, behavioral, and biomedical sciences. Behavior Research Methods 2007;39:175–91. https://doi.org/10.3758/BF03193146.

[28] Chase HW, Swainson R, Durham L, Benham L, Cools R. Feedback-related Negativity Codes Prediction Error but Not Behavioral Adjustment during Probabilistic Reversal Learning. Journal of Cognitive Neuroscience 2011;23:936–46. https://doi.org/10.1162/jocn.2010.21456.

[29] Warren CM, Hyman JM, Seamans JK, Holroyd CB. Feedback-related negativity observed in rodent anterior cingulate cortex. Journal of Physiology-Paris 2015;109:87–94. https://doi.org/10.1016/j.jphysparis.2014.08.008.

[30] Smith EH, Horga G, Yates MJ, Mikell CB, Banks GP, Pathak YJ, et al. Widespread temporal coding of cognitive control in the human prefrontal cortex. Nat Neurosci 2019;22:1883–91. https://doi.org/10.1038/s41593-019-0494-0.

[31] Ma L, Chan JL, Johnston K, Lomber SG, Everling S. Macaque anterior cingulate cortex deactivation impairs performance and alters lateral prefrontal oscillatory activities in a rule-switching task. PLoS Biol 2019;17:e3000045. https://doi.org/10.1371/journal.pbio.3000045.

[32] Donkers FCL, Nieuwenhuis S, Van Boxtel GJM. Mediofrontal negativities in the absence of responding. Cognitive Brain Research 2005;25:777–87. https://doi.org/10.1016/j.cogbrainres.2005.09.007.

[33] Brunia CHM, Hackley SA, Van Boxtel GJM, Kotani Y, Ohgami Y. Waiting to perceive: Reward or punishment? Clinical Neurophysiology 2011;122:858–68. https://doi.org/10.1016/j.clinph.2010.12.039.

[34] Ohgami Y, Kotani Y, Hiraku S, Aihara Y, Ishii M. Effects of reward and stimulus modality

on stimulus-preceding negativity. Psychophysiology 2004;41:729–38. https://doi.org/10.1111/j.1469-8986.2004.00203.x.

[35] Reinhart RMG, Woodman GF. Causal Control of Medial–Frontal Cortex Governs Electrophysiological and Behavioral Indices of Performance Monitoring and Learning. J Neurosci 2014;34:4214–27. https://doi.org/10.1523/JNEUROSCI.5421-13.2014.

[36] Haber SN, Knutson B. The Reward Circuit: Linking Primate Anatomy and Human Imaging. Neuropsychopharmacol 2010;35:4–26. https://doi.org/10.1038/npp.2009.129.

Figure Legends

Figure 1. Experimental design and procedure. Eligible participants proceeded to a pre-test session of a food incentive delay task with concurrent EEG recording. Participants were then randomly assigned to receive either active theta-band transcranial temporal interference stimulation (tTIS; n = 17) or sham stimulation (n = 17) for 20 minutes. Following stimulation, all participants completed a post-test session identical to the pre-test. Both pre-test and post-test sessions lasted approximately 40 minutes.

Figure 2. Experimental task design scheme. (A) Practice session. Participants completed a brief practice version of the incentive delay task using natural reward stimuli. Practice ended when accuracy reached ≥ 0.80 within one cycle. (B) Food incentive delay task. Each trial began with a fixation cross followed by a food cue (1500 ms) indicating reward probability (80% high vs. 20% low). Participants then reported reward expectation via key press (self-paced), followed by a 2000-ms delay and outcome presentation (1500 ms; food image vs. scrambled image). Inter-trial intervals were jittered between 350 and 650 ms. Each pre- and post-stimulation phase consisted of 150 trials, divided into three blocks of 50 trials with short breaks between blocks.

Figure 3. Electric-field simulations of the stimulation montage. (A) tTIS simulation using the experimental montage. The first pair of electrodes was placed at AF3 and Fz, while the second pair was placed at CP3 and F7. The injected current was set at 1.6 mA (peak to baseline) per electrode. (B) tDCS simulation using the same electrode placement and current intensity, shown for comparison.

Figure 4. Trial-level FRN amplitudes as a function of behavioral prediction error category. Scatterplots show single-trial FRN amplitudes (μV) across behavioral prediction error categories (PE = −1, 0, +1), separately for the active and sham groups in the pre- and post-stimulation phases. Lines indicate fitted trial-level relationships shown for visualization.

Figure 5. Trial-level FRN amplitudes as a function of model-derived prediction errors.

Scatterplots show single-trial FRN amplitudes (μV) as a function of Rescorla–Wagner model-derived prediction errors (PE_RW), separately for the active and sham groups in the pre- and post-stimulation phases. Lines indicate fitted trial-level relationships shown for visualization.

Figure 6. FRN elicited by food reward outcomes before and after stimulation. Grand-average ERP waveforms at FCz (top) and corresponding scalp topographies (bottom) are shown for the active tTIS group (left) and the sham group (right), separately for the pre- and post-stimulation phases. FRN was quantified as the peak negativity within the 250–350 ms time window following feedback onset (highlighted in gray). Waveforms are time-locked to feedback onset (0 ms) and plotted with pre-stimulation in red and post-stimulation in blue. Topographies depict mean amplitude within the FRN time window.

Figure 7. SPN during anticipation of food reward outcomes before and after stimulation. Grand-average SPN waveforms and scalp topographies are shown for the active tTIS group (left) and the sham group (right), separately for the pre- and post-stimulation phases. SPN was quantified as mean amplitude during the −200 to 0 ms interval prior to feedback onset (highlighted in gray). Waveforms are time-locked to feedback onset (0 ms) and plotted with pre-stimulation in red and post-stimulation in blue. Topographies depict mean amplitude within the SPN measurement window.

Figure 8. Quantitative ERP results for feedback evaluation and anticipation. (A) FRN amplitudes elicited by food reward feedback at FCz (250–350 ms), shown separately for the sham and active tTIS groups before (Pre) and after (Post) stimulation. (B) SPN amplitudes during the anticipatory period (−200 to 0 ms) prior to feedback onset. Bars represent group means (± SEM), and dots represent individual participants. Significance is denoted as $p < .01$ (**); *ns*, non-significant.

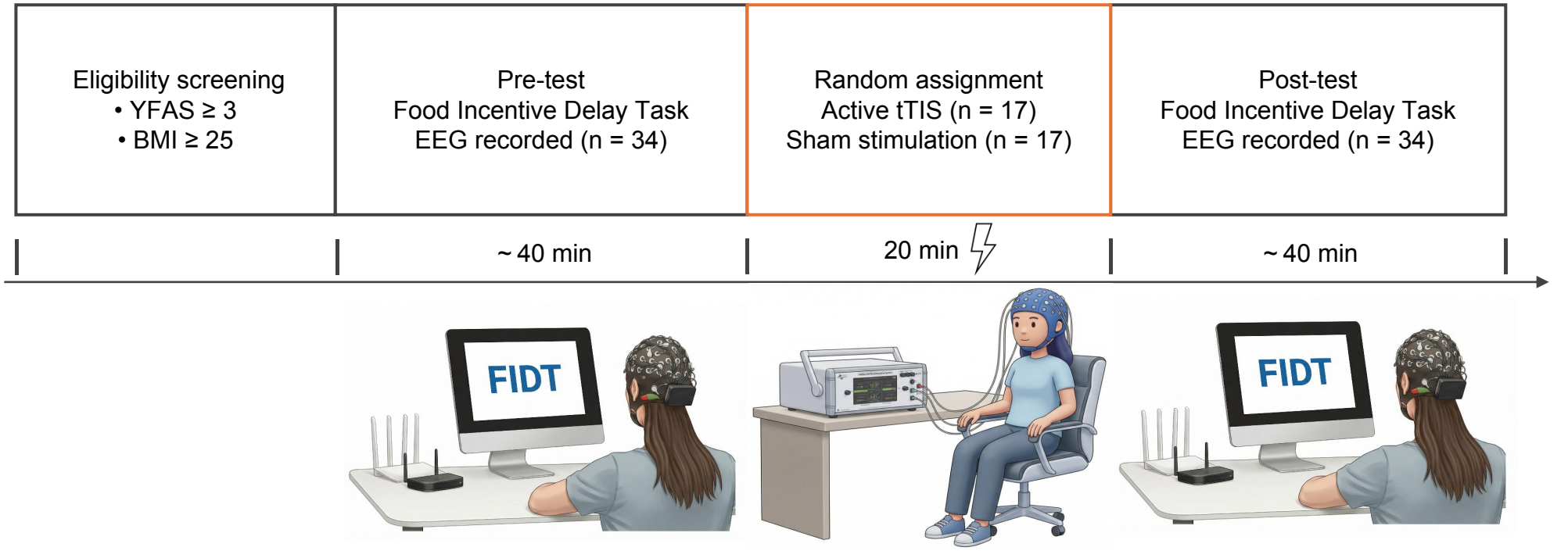
Eligibility screening
• YFAS ≥ 3
• BMI ≥ 25
Pre-test
Food Incentive Delay Task
EEG recorded (n = 34)
Random assignment
Active tTIS (n = 17)
Sham stimulation (n = 17)
Post-test
Food Incentive Delay Task
EEG recorded (n = 34)
~ 40 min
20 min
~ 40 min
FIDT
FIDT

A: Practice

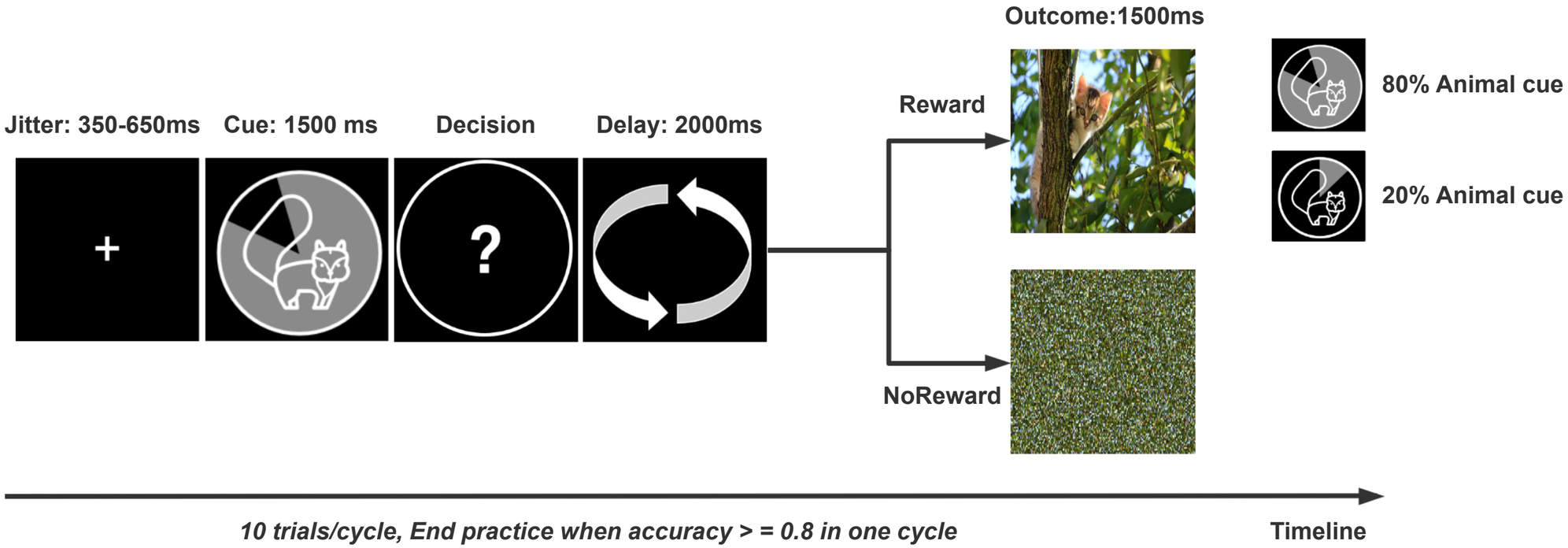

B: Food incentive delay task

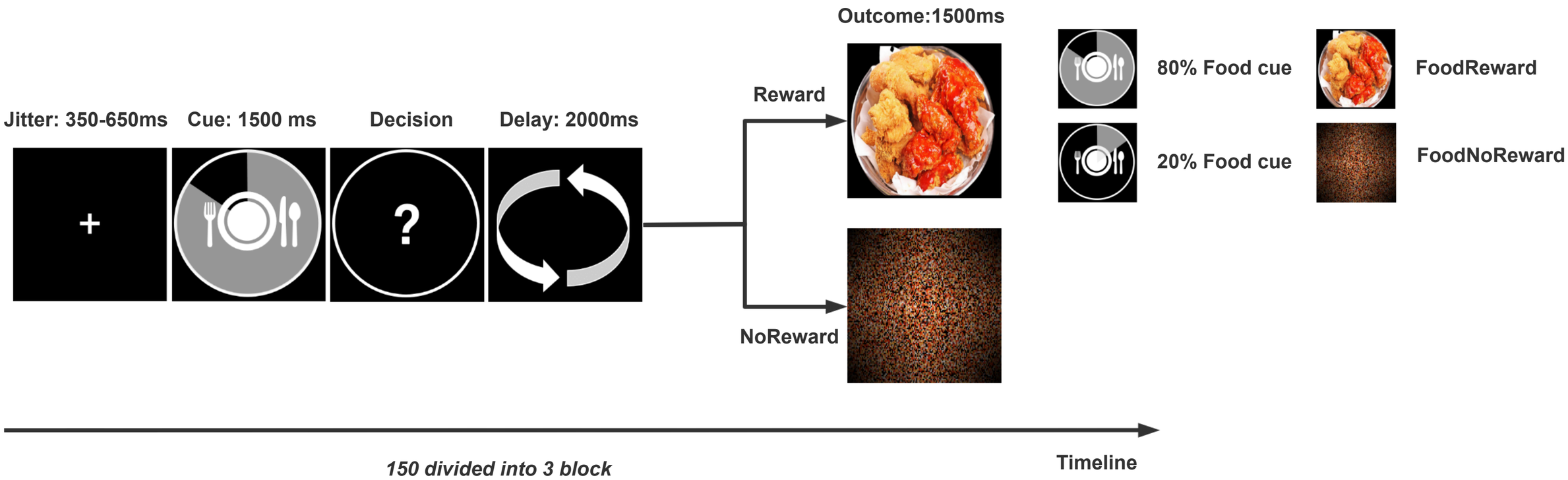

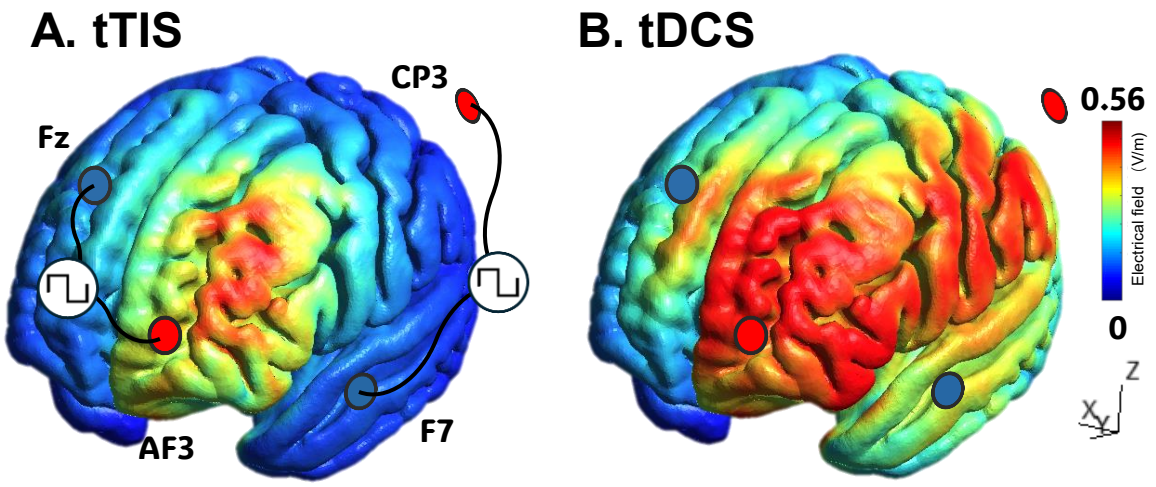
A. tTIS
CP3
Fz
AF3
F7
B. tDCS
0.56
Electrical field (V/m)
0
Z
X
Y

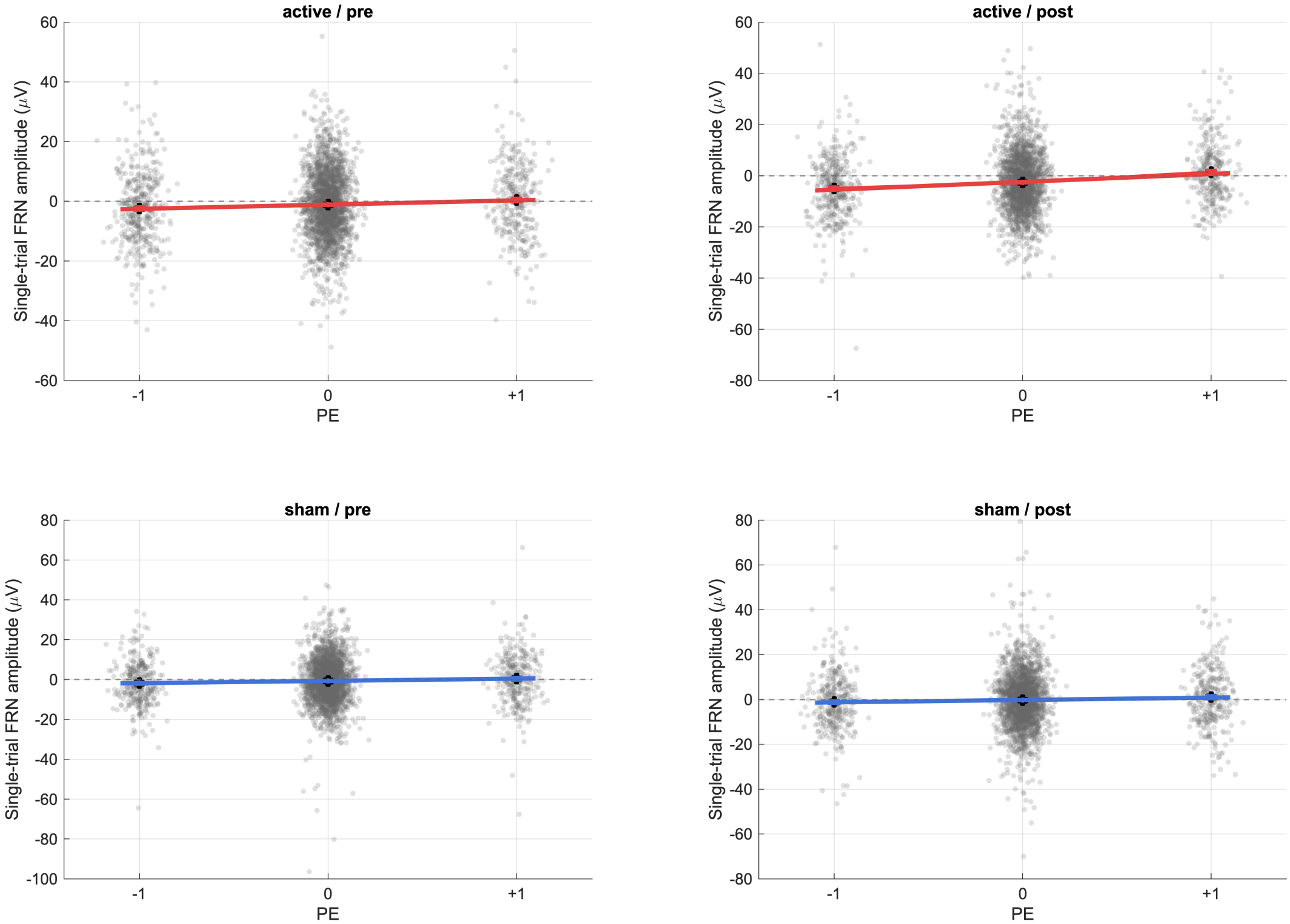
active / pre
active / post
sham / pre
sham / post
Single-trial FRN amplitude (μV)
PE
-1
0
+1
60
40
20
0
-20
-40
-60
-80
-100

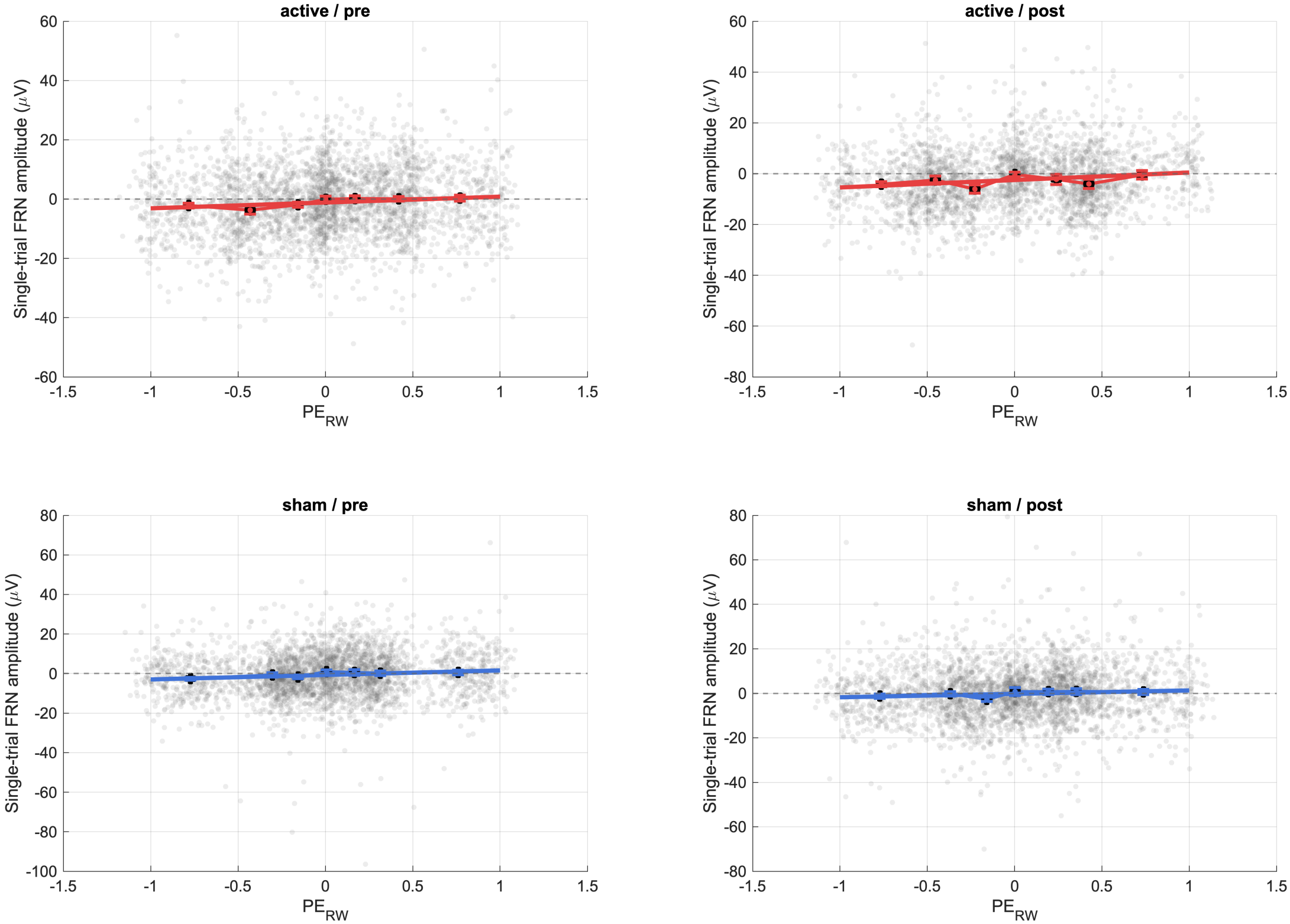
active / pre
active / post
sham / pre
sham / post
Single-trial FRN amplitude (μV)
PE_{RW}
60
40
20
0
-20
-40
-60
-80
-100
-1.5
-1
-0.5
0
0.5
1
1.5

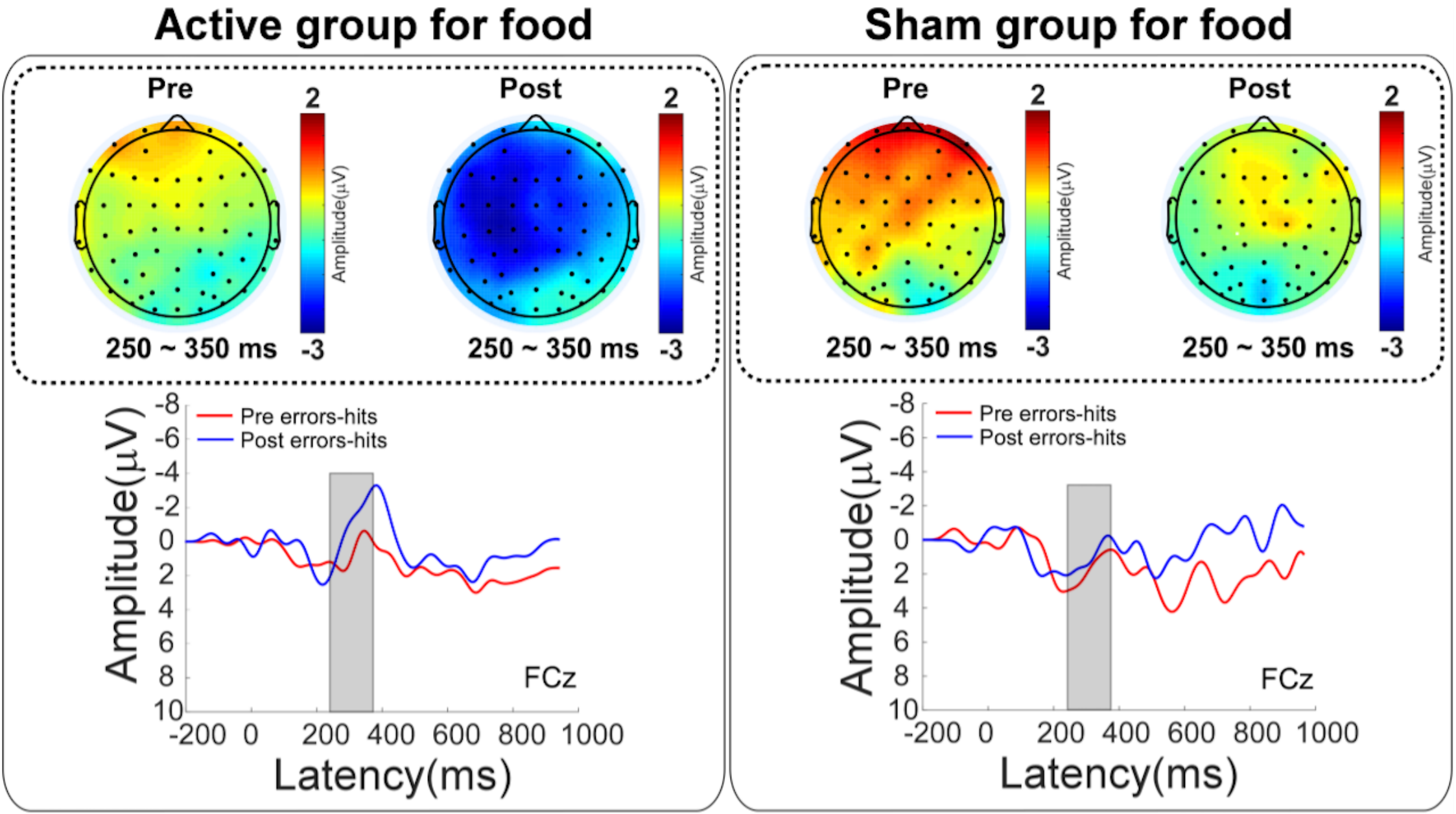
Active group for food
Sham group for food
Pre
Post
2
-3
Amplitude(μV)
250 ~ 350 ms
Pre errors-hits
Post errors-hits
FCz
Amplitude(μV)
Latency(ms)
-8
-6
-4
-2
0
2
4
6
8
10
-200
0
200
400
600
800
1000

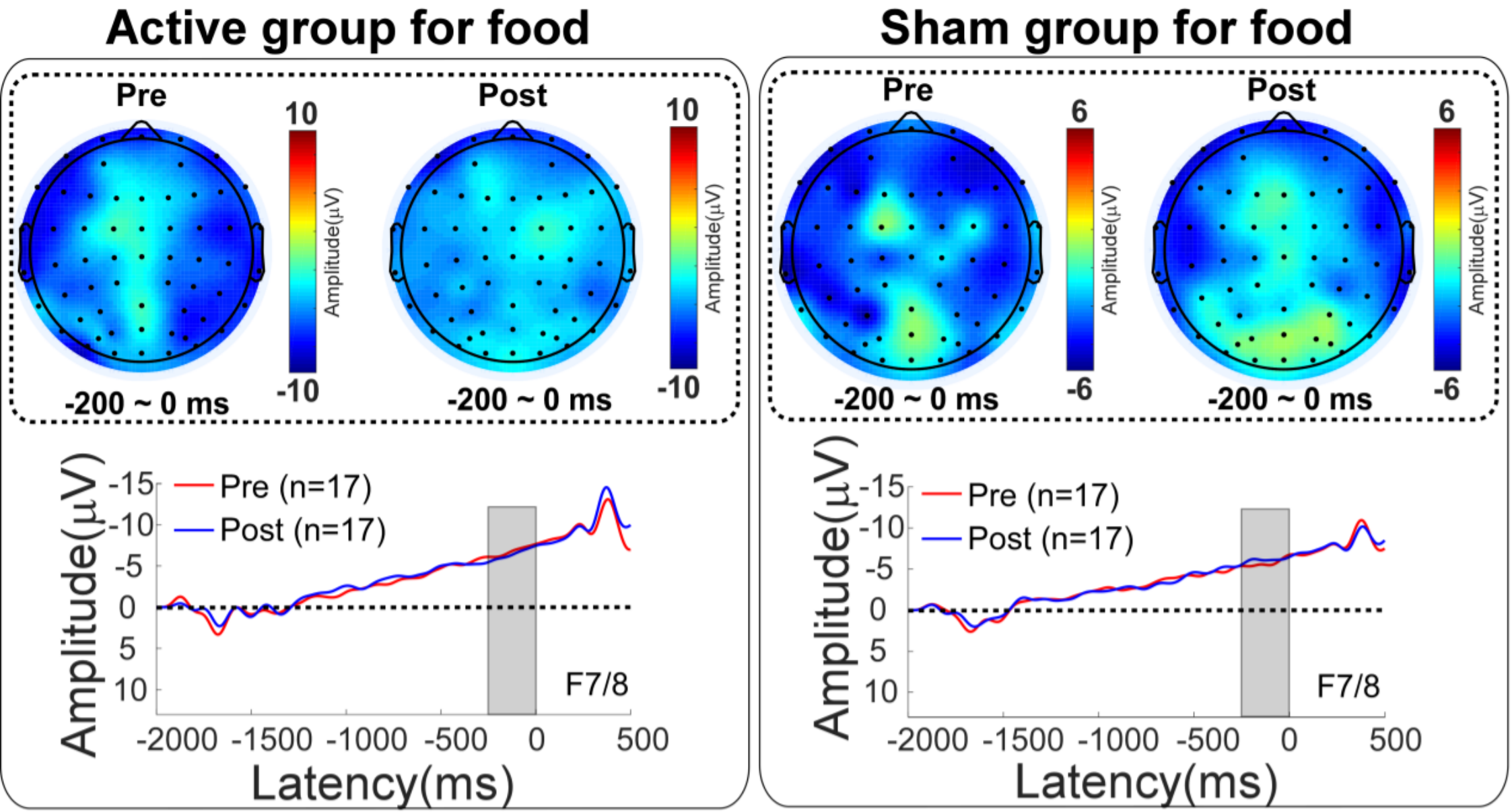
Active group for food
Pre
Post
10
-10
Amplitude(μV)
-200 ~ 0 ms
Pre (n=17)
Post (n=17)
F7/8
Amplitude(μV)
Latency(ms)
Sham group for food
6
-6

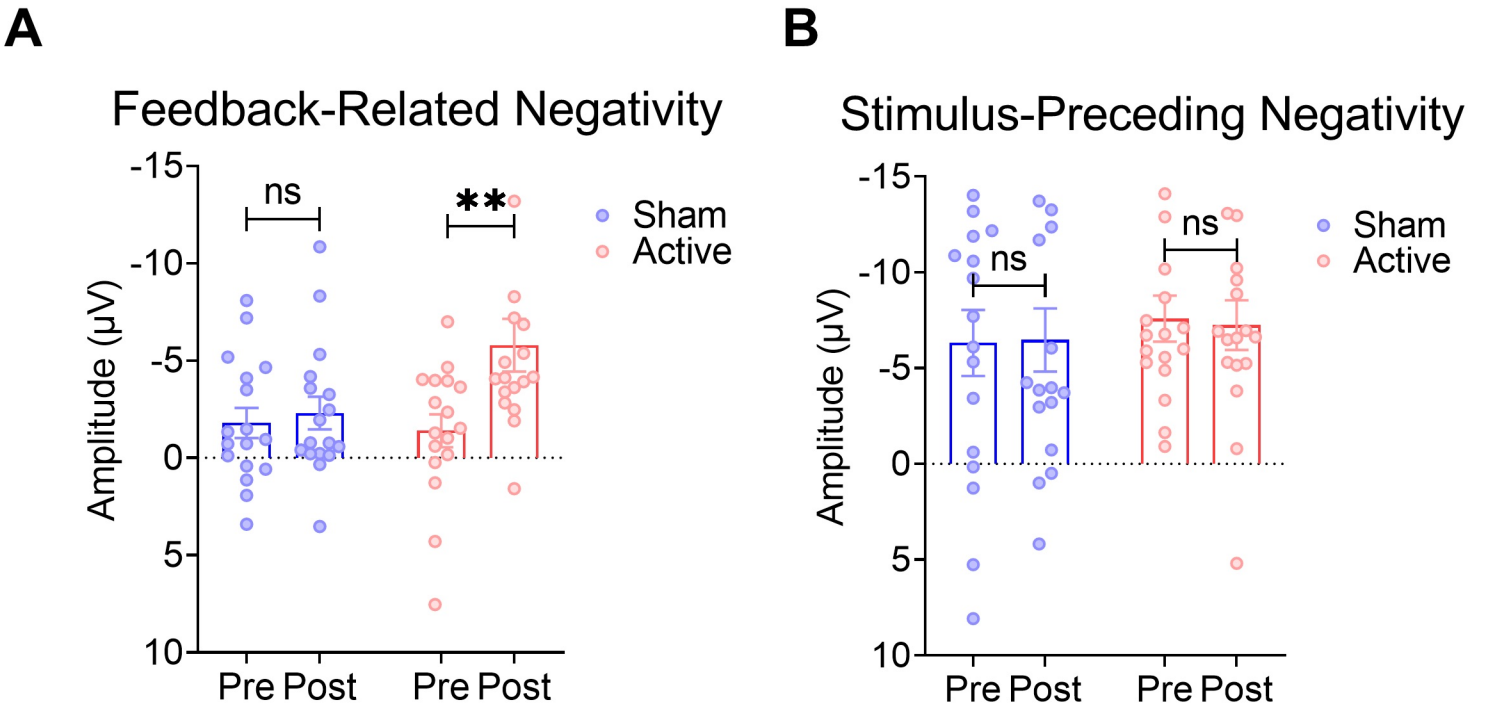
A
Feedback-Related Negativity
Amplitude (μV)
-15
-10
-5
0
5
10
ns
**
Sham
Active
Pre Post
Pre Post
B
Stimulus-Preceding Negativity
Amplitude (μV)
-15
-10
-5
0
5
10
ns
ns
Sham
Active
Pre Post
Pre Post

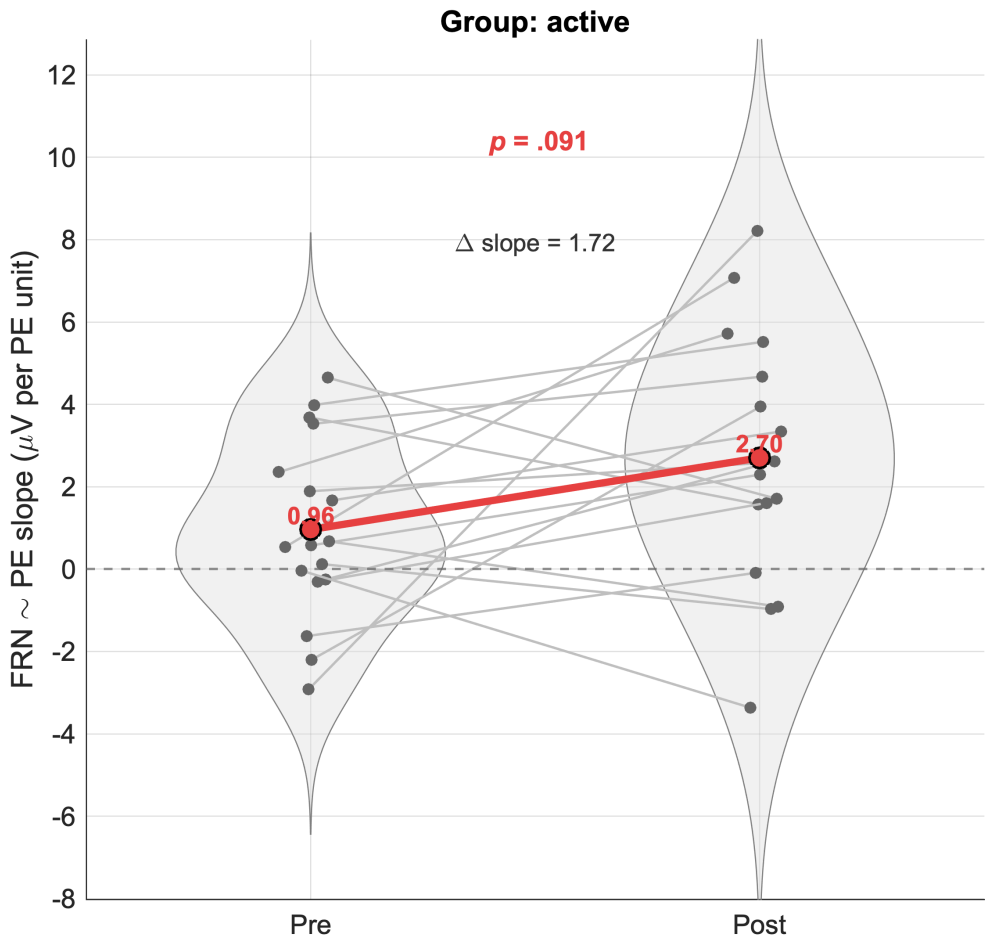
Group: active
p = .091
Δ slope = 1.72
0.96
2.70
FRN ~ PE slope (μV per PE unit)
12
10
8
6
4
2
0
-2
-4
-6
-8
Pre
Post

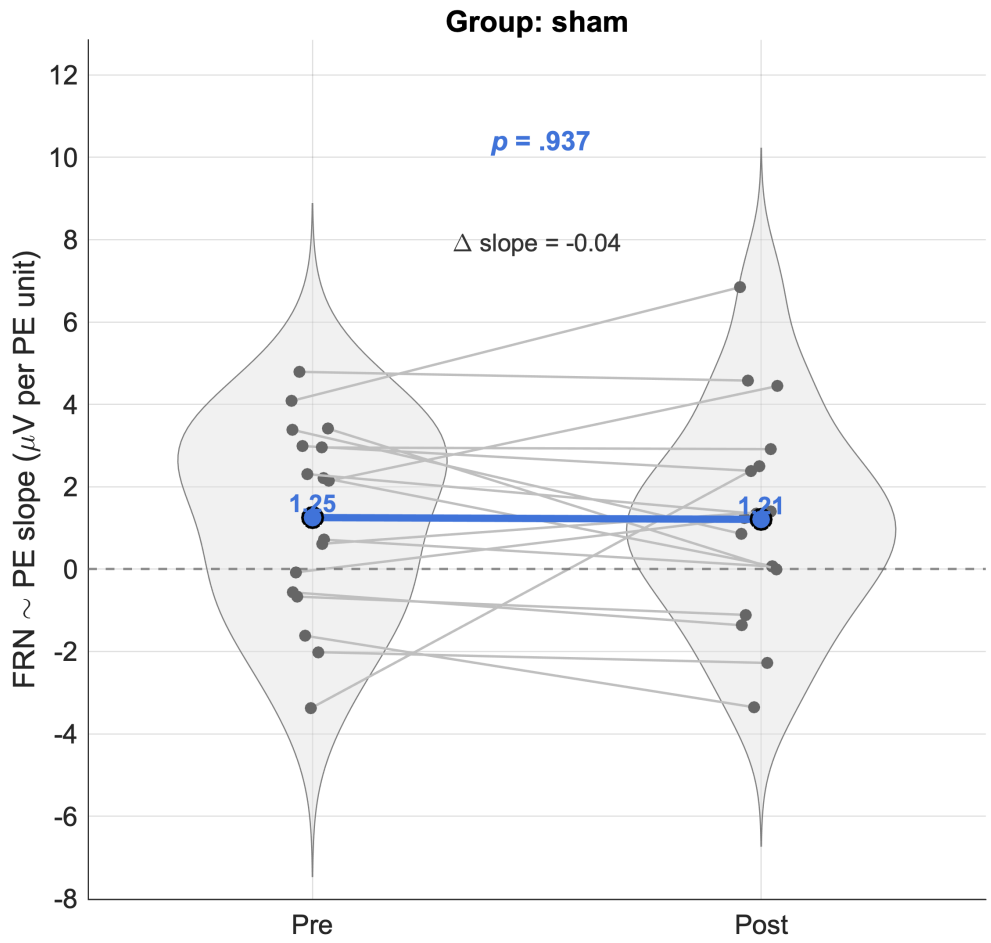
Group: sham
p = .937
Δ slope = -0.04
1.25
1.21
FRN ~ PE slope (μV per PE unit)
12
10
8
6
4
2
0
-2
-4
-6
-8
Pre
Post

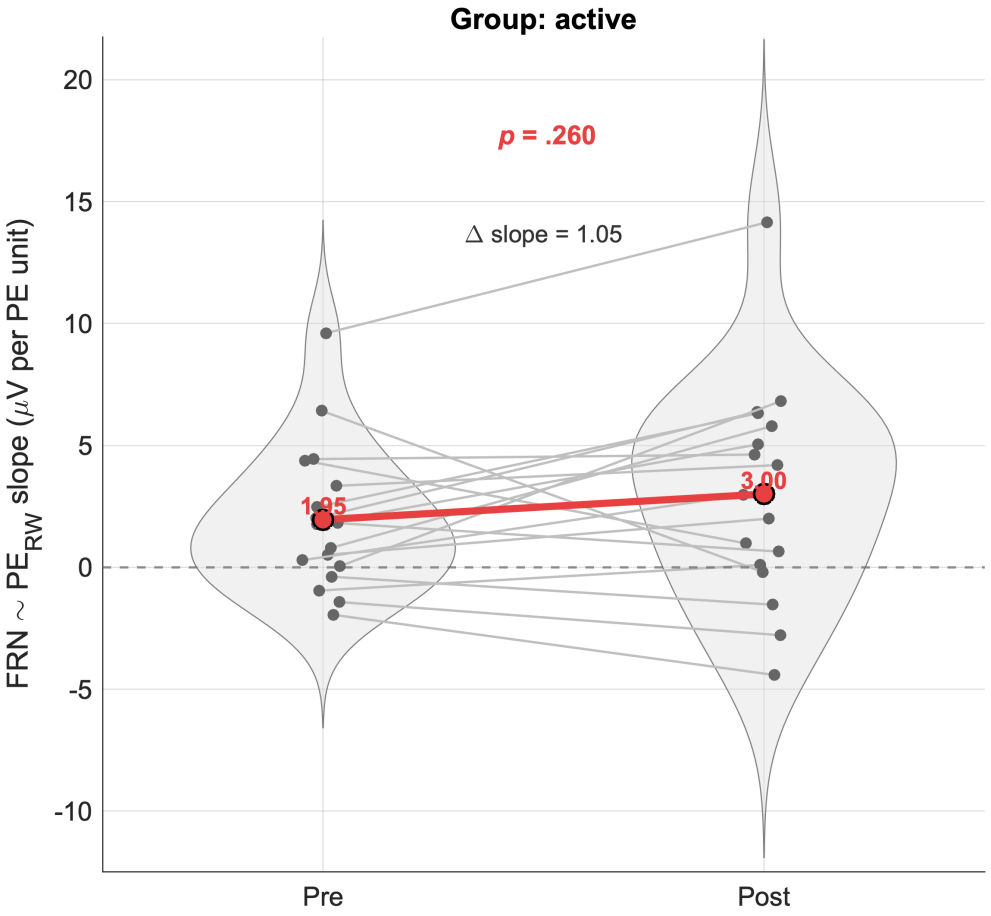
Group: active
p = .260
Δ slope = 1.05
1.95
3.00
20
15
10
5
0
-5
-10
FRN ~ PE_RW slope (μV per PE unit)
Pre
Post

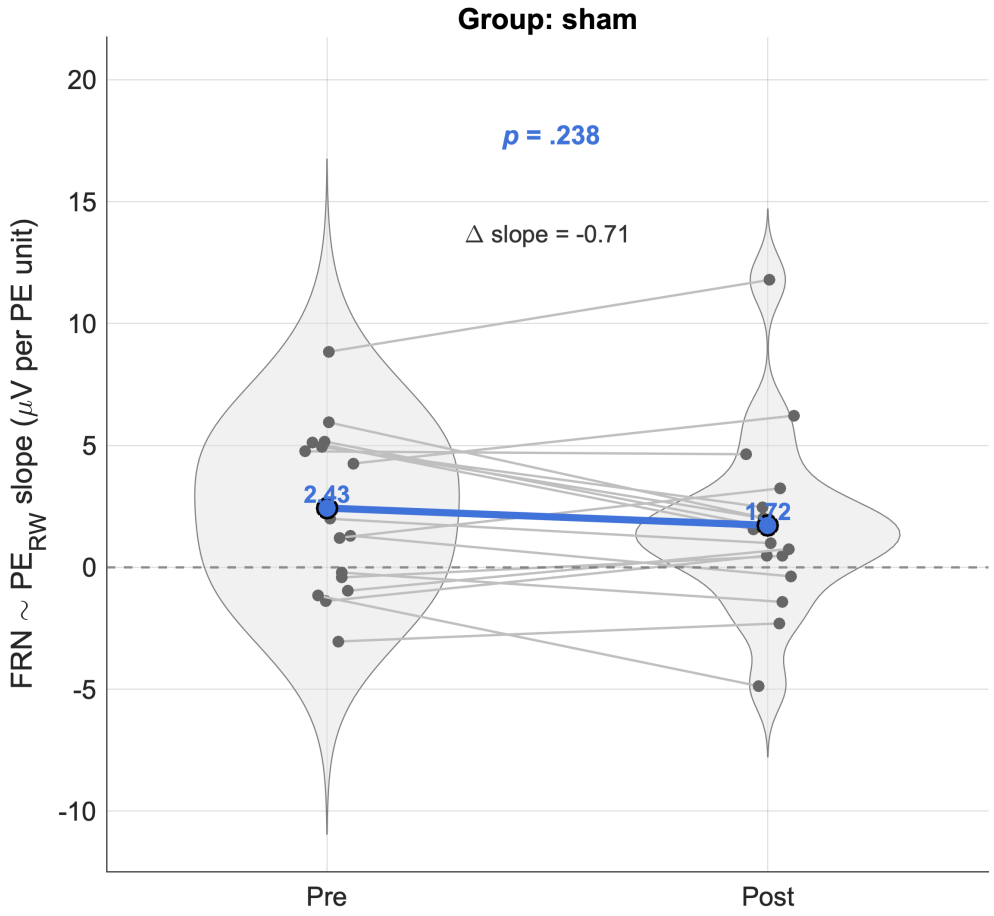
Group: sham
p = .238
Δ slope = -0.71
2.43
1.72
20
15
10
5
0
-5
-10
FRN ~ PE_RW slope (μV per PE unit)
Pre
Post

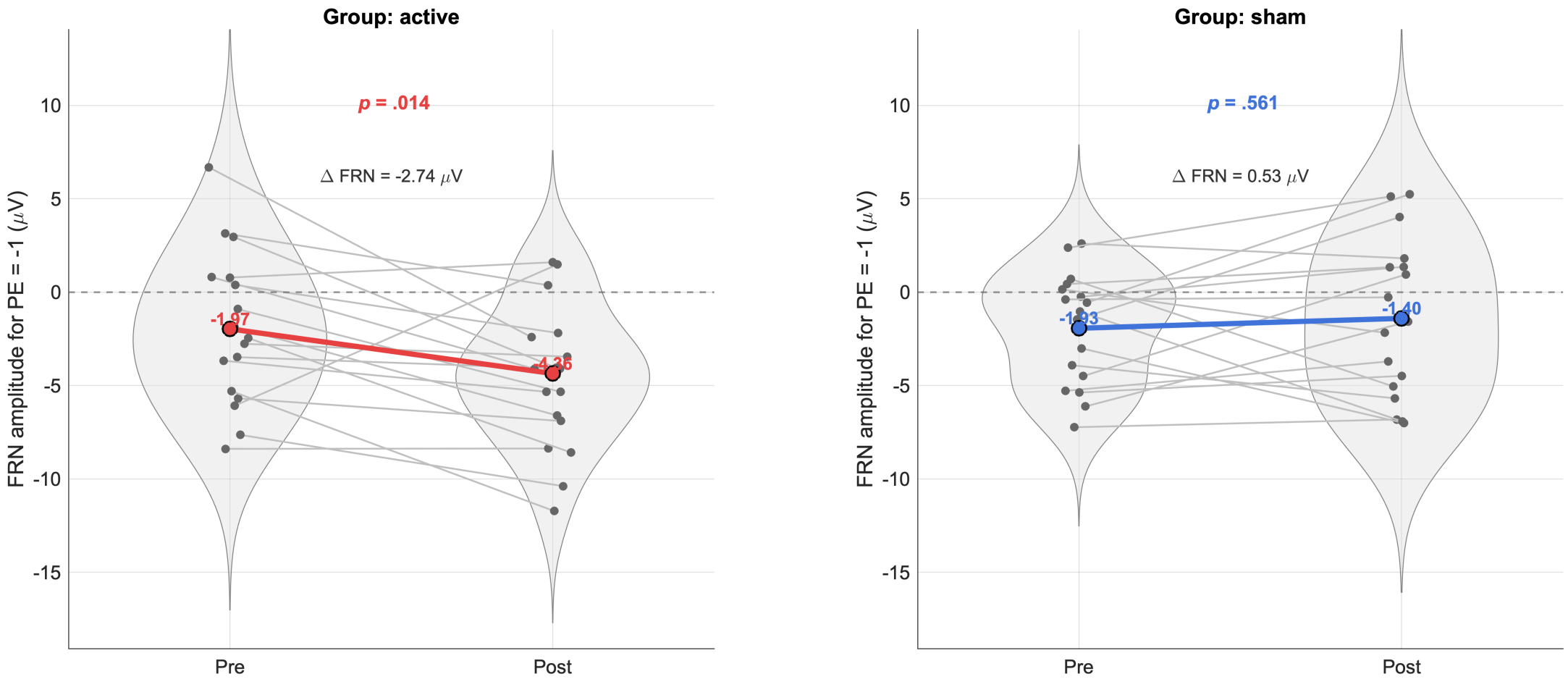
Group: active
p = .014
Δ FRN = -2.74 μV
-1.97
-4.36
FRN amplitude for PE = -1 (μV)
10
5
0
-5
-10
-15
Pre
Post
Group: sham
p = .561
Δ FRN = 0.53 μV
-1.93
-1.40
FRN amplitude for PE = -1 (μV)
10
5
0
-5
-10
-15
Pre
Post

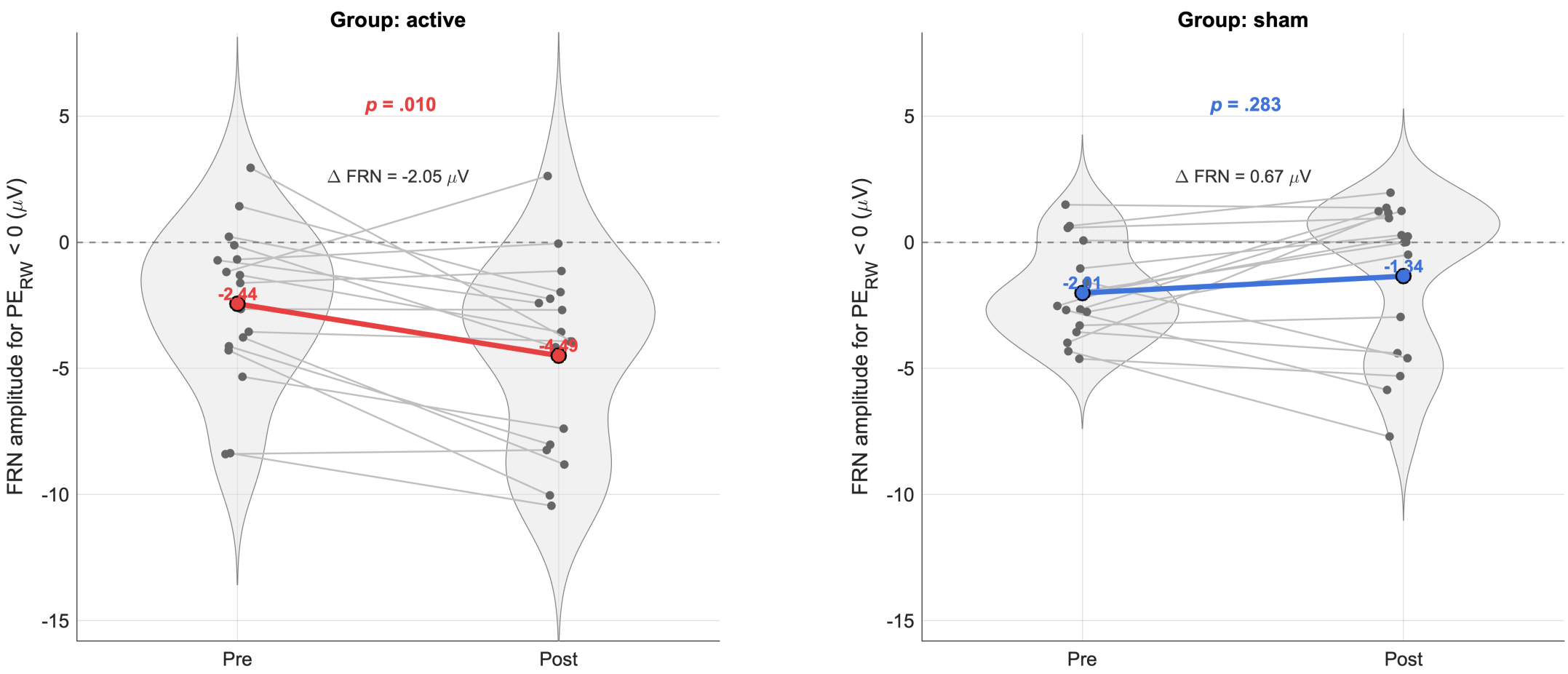
Group: active
p = .010
Δ FRN = -2.05 μV
-2.44
-4.49
FRN amplitude for PE_RW < 0 (μV)
5
0
-5
-10
-15
Pre
Post
Group: sham
p = .283
Δ FRN = 0.67 μV
-2.01
-1.34
FRN amplitude for PE_RW < 0 (μV)
5
0
-5
-10
-15
Pre
Post